

ACTIVE GALACTIC NUCLEI WITH CANDIDATE INTERMEDIATE-MASS BLACK HOLES

JENNY E. GREENE

Harvard-Smithsonian Center for Astrophysics, 60 Garden Street, Cambridge, MA 02138

AND

LUIS C. HO

The Observatories of the Carnegie Institution of Washington, 813 Santa Barbara Street, Pasadena, CA 91101-1292

Received 2004 February 29; accepted 2004 April 5

ABSTRACT

We present an initial sample of 19 intermediate-mass black hole candidates in active galactic nuclei culled from the first data release of the Sloan Digital Sky Survey. Using the line width–luminosity mass scaling relation established for broad-line active nuclei, we estimate black hole masses in the range of $M_{\text{BH}} \approx 8 \times (10^4 - 10^6) M_{\odot}$, a regime in which only two objects are currently known. The absolute magnitudes are faint for active galactic nuclei, ranging from $M_g \approx -15$ to -18 mag, while the bolometric luminosities are all close to the Eddington limit. The entire sample formally satisfies the line width criterion for so-called narrow-line Seyfert 1 galaxies; however, they display a wider range of Fe II and [O III] $\lambda 5007$ line strengths than is typically observed in this class of objects. Although the available imaging data are of insufficient quality to ascertain the detailed morphologies of the host galaxies, it is likely that the majority of the hosts are relatively late-type systems. The host galaxies have estimated g -band luminosities ~ 1 mag fainter than M^* for the general galaxy population at $z \approx 0.1$. Beyond simply extending the known mass range of central black holes in galactic nuclei, these objects provide unique observational constraints on the progenitors of supermassive black holes. They are also expected to contribute significantly to the integrated signal for future gravitational wave experiments.

Subject headings: galaxies: active — galaxies: nuclei — galaxies: Seyfert

1. INTRODUCTION

Dynamical studies have established the existence of supermassive black holes (BHs) with masses $M_{\text{BH}} \approx 10^6 - 10^9 M_{\odot}$ in the centers of most, if not all, local galaxies with bulges (Magorrian et al. 1998; Richstone 2004). A significant challenge to any model of cosmological BH growth is the nature of seed BHs. Observations of intermediate-mass BHs ($M_{\text{BH}} \approx 10^3 - 10^6 M_{\odot}$) in the local universe would provide the most direct empirical constraints on such seeds. The $M_{\text{BH}} - \sigma_*$ relation (Ferrarese & Merritt 2000; Gebhardt et al. 2000a; Tremaine et al. 2002) strongly indicates feedback in the coevolution of galaxies and BHs, but it is still an open question whether the relation is established at early or late times. If, as some models suggest (e.g., Di Matteo et al. 2003), the $M_{\text{BH}} - \sigma_*$ relation is established late in the evolution of a galaxy, then we may expect to see deviations from this relation in a population of intermediate-mass BHs that is not yet fully grown. There are other motivations to characterize the lowest end of the nuclear BH mass distribution. Certainly their number and mass distribution will impact the expected integrated background in gravitational radiation (e.g., Hughes 2002). Presumably they will pass through an active phase of accretion and contribute at some level to the observed integrated background radiation, particularly at X-ray energies. The range of accretion phenomena they display will depend on the major accretion modes for BHs of such low mass. The accretion states and, by extension, radiative growth mechanisms of this population will therefore have direct implications for the growth history of primordial BHs. Apart from their physical implications, intermediate-mass BHs have practical value in that they offer tremendous leverage in anchoring local BH-galaxy scaling correlations such as the $M_{\text{BH}} - \sigma_*$ relation.

Recently discovered intermediate-mass BH candidates in galactic nuclei offer tantalizing hints as to the nature of this population. NGC 4395 is a very late-type (Sdm) spiral with no bulge component, whose central stellar velocity dispersion is $\sigma_* < 30 \text{ km s}^{-1}$ (Filippenko & Ho 2003). Nevertheless, it has the emission properties of a type 1 active galactic nucleus (AGN), with broad permitted optical and UV emission lines (Filippenko & Sargent 1989; Filippenko et al. 1993), a compact radio core (Ho & Ulvestad 2001) with a nonthermal brightness temperature (Wrobel et al. 2001), and a pointlike, hard X-ray source (Ho et al. 2001) that is highly variable (Moran et al. 1999, 2004; Shih et al. 2003). Mass estimates based on the $H\beta$ line width–luminosity mass scaling relation and X-ray variability suggest a BH mass of $10^4 - 10^5 M_{\odot}$ (Filippenko & Ho 2003). Interestingly, these agree with the limit of less than $10^5 M_{\odot}$ derived from the $M_{\text{BH}} - \sigma_*$ relation (Filippenko & Ho 2003). POX 52, on the other hand, has a dwarf elliptical host. Recently revisited by Barth et al. (2004), POX 52 was first observed by Kunth et al. (1987), who noted the Seyfert-like characteristics of its optical spectrum, including a broad component to the $H\beta$ emission line. The galaxy has a central velocity dispersion of 36 km s^{-1} , which yields a mass estimate of $M_{\text{BH}} = 1.4 \times 10^5 M_{\odot}$, again consistent with the value of $1.6 \times 10^5 M_{\odot}$ derived from the $H\beta$ line width–luminosity mass scaling relation. The [O III] $\lambda 5007$ line width, $\sigma \approx 37 \text{ km s}^{-1}$, is also fully consistent with the stellar velocity dispersion (Barth et al. 2004).

Unfortunately, it is currently technically impossible to obtain direct mass measurements for $M_{\text{BH}} \lesssim 10^6 M_{\odot}$ because of our inability to resolve the BH sphere of influence, for all but the nearest galaxies in the Local Group (e.g., M33; Gebhardt et al. 2001). The only direct mass determinations for intermediate-mass BHs come from observations of massive star clusters

(Gebhardt et al. 2002; Gerssen et al. 2002), which, in any case, have been controversial (Baumgardt et al. 2003a, 2003b). Barring evidence from spatially resolved kinematics, the best indicator for nuclear BHs in nearby galaxies comes from AGN activity as revealed through optical emission-line intensity ratios (Baldwin et al. 1981; Veilleux & Osterbrock 1987; Ho et al. 1993), kinematically distinct, broad emission lines (e.g., Ho et al. 1997c), or the presence of compact, nonstellar radio and X-ray cores (e.g., Ho et al. 2001; Nagar et al. 2002; Terashima & Wilson 2003; see Ho 2004a for a review).

Thus, the best hope to find intermediate-mass BHs is through an AGN survey. However, there are at least two practical challenges. First, it may be that objects like NGC 4395 are quite rare. In the Palomar survey of ~ 500 nearby galaxies, NGC 4395 is the only example of its kind found (Ho et al. 1997a, 1997b). POX 52 was discovered serendipitously in a fairly limited objective prism survey for emission-line objects (Kunth et al. 1987). These two are the only known cases of intermediate-mass BHs in galactic nuclei. Thus, to accumulate a significant sample will require a much larger survey. Second, even radiative signatures of accretion in these objects will be challenging to uncover. The host galaxies are expected to be either very late-type systems with low mass and therefore intrinsically faint, or else regular, luminous disk-dominated galaxies with a tiny or nonexistent bulge. Even at a high accretion rate a $10^5 M_\odot$ BH will itself have a low luminosity. As a result, detection of the faint AGN will be limited by sensitivity and host galaxy contamination.

A large-area, sensitive, and uniform optical spectroscopic galaxy survey, such as the Sloan Digital Sky Survey (SDSS; York et al. 2000), offers the best opportunity for finding a significant number of new intermediate-mass BH candidates. We present the first sample of candidates culled from the SDSS. We discuss the data in § 2, the sample definition and analysis in § 3, and the main results in § 4. In this paper we assume the following cosmological parameters to derive distances: $H_0 = 100 h = 72 \text{ km s}^{-1} \text{ Mpc}^{-1}$, $\Omega_m = 0.3$, and $\Omega_\Lambda = 0.7$.

2. THE SDSS DATA

Since we have relied heavily on the SDSS software pipeline, we will briefly discuss relevant characteristics of the survey. This is by no means a complete discussion. Details of SDSS photometry and spectroscopy can be found in the Early Data Release (EDR; Stoughton et al. 2002) and Data Release One (DR1; Abazajian et al. 2003).

The SDSS uses a dedicated 2.5 m telescope to image one-quarter of the sky and obtain follow-up spectroscopy on automatically selected star, galaxy, and quasar candidates. The DR1 includes a photometric sample of 53 million objects over 2099 deg^2 and photometrically defined quasar, galaxy, and stellar spectra over 1360 deg^2 (Abazajian et al. 2003).

Calibration and sample selection for both surveys is conducted by automated pipelines. The photometric pipeline, *Photo*, performs bias subtraction, flat-fielding, cosmic-ray rejection, and masking of bad pixels, followed by astrometry, point-spread function modeling, object identification, and image deblending. It measures four different ($a \sinh$) magnitudes (Lupton et al. 1999). The Petrosian magnitude, measured within a radius defined by the shape of the azimuthally averaged light profile of the galaxy, is best for photometry of extended objects such as galaxies (Stoughton et al. 2002). Typical photometric calibration errors are 0.02 mag in g (Smith et al. 2002), while the zero points between the SDSS

and AB magnitude system could differ by as much as 10% (Stoughton et al. 2002).

Galaxy targets are automatically selected based on morphology. Specifically, resolved sources with $r \lesssim 17.77$ mag are targeted as galaxies (note that this cutoff varied between the EDR and the DR1). Candidates with magnitudes brighter than 15 in g or r or 14.5 in i are rejected in case of contamination of other fibers. A surface brightness cut is also applied, and targets may be excluded as a result of proximity because the fiber holders have a finite size and are kept $55''$ apart from each other to avoid fiber collisions. Quasar candidates are selected on the basis of a color selection technique detailed in Richards et al. (2002).

SDSS spectra are acquired with a pair of double, fiber-fed spectrographs. A plate of 3 deg^2 with 640 optical fibers is drilled for each field. Each fiber subtends a diameter of $3''$, corresponding to $\sim 6.5 \text{ kpc}$ at $z = 0.1$. The spectra have an instrumental resolution of $\lambda/\Delta\lambda \approx 1800$ ($\sigma_{\text{ins}} \approx 71 \text{ km s}^{-1}$). Integration times are determined for a minimum signal-to-noise ratio (S/N) of 4 at $g = 20.2$ mag. The spectroscopic pipeline performs basic calibration as above, as well as spectral extraction, sky subtraction, removal of atmospheric absorption bands, and wavelength and spectrophotometric calibration. Redshifts are determined using χ^2 fits to stellar, emission-line galaxy, and quasar templates, as well as to the emission lines themselves; the typical accuracy is $\sim 30 \text{ km s}^{-1}$.

3. THE SAMPLE AND ANALYSIS

Our primary sample was culled from a parent sample of broad-line AGNs at $z \leq 0.35$ in the DR1. These are unambiguous AGN candidates with virial BH mass estimates $\leq 10^6 M_\odot$, which hereafter we consider to be the upper bound for intermediate-mass BHs. We determine “virial” BH masses using a variant of the line width–luminosity mass scaling relation of Kaspi et al. (2000), whose robustness has been tested with respect to the $M_{\text{BH}}\text{-}\sigma_*$ relation of inactive galaxies (Gebhardt et al. 2000b; Ferrarese et al. 2001; see Barth 2004 for a review). In order to apply this method, we first identify all the AGNs from DR1 that have a broad component to at least the $\text{H}\alpha$ emission line. In order to detect objects with weak lines and to reliably measure emission-line and continuum parameters, we must properly remove the contaminating starlight from the host galaxy, model the profiles of the emission lines, and quantify the strength of the AGN continuum luminosity. We discuss these various steps below.

3.1. Starlight and Continuum Subtraction

Low-luminosity AGNs are challenging to detect because the signature emission lines are often contaminated by starlight. The SDSS fibers always include significant host galaxy emission, making careful removal of the stellar continuum essential to reliably measure the emission-line spectrum, and especially to detect any weak, broad features. Because we expect $\text{H}\alpha$ to be the strongest permitted line in the optical, and hence best suited for detecting a broad-line component if present, we start with the $\sim 153,000$ galaxies and quasars in the DR1 with $z \leq 0.35$.

The next step is to remove the starlight, along with any additional featureless nonstellar continuum emission, in order to produce a pure emission-line spectrum. A variety of template-fitting techniques exist to accomplish this (see, e.g., Ho 2004a for a review). For this work we use a principal component analysis (PCA) algorithm adopted from Hao &

Strauss (2004; see also Connolly & Szalay 1999). Assuming a linear relation between all spectral variations, PCA (or the Karhunen-Loève transform) transforms a large library of input spectra to an orthogonal basis in which each eigenspectrum is along a direction of maximal variance. The input spectra are derived from absorption-line spectra from the SDSS, and an A-star spectrum may be included to account for a post-starburst stellar population. Each program spectrum is then modeled as a linear combination of the eigenspectra. The PCA technique has a number of benefits when a large, homogeneous database like SDSS is available. The method typically requires no more than eight eigenspectra to fully reconstruct a given galaxy spectrum, and for absorption-line galaxies the resulting solution is unique. Furthermore, the eigenvectors naturally include variance in velocity dispersion as long as the template galaxies span the same range as the target sample. In practice, some galaxies contain substantial nonstellar continuum emission, which we model as a power law fixed to a slope of $\beta = 1.0$, where $f_\lambda \propto \lambda^{-\beta}$. As discussed in J. E. Greene & L. C. Ho (2004, in preparation), the AGN-dominated objects in our sample typically have a power-law continuum spectrum with this slope.

Examples of spectra before and after starlight and continuum subtraction are given in the left panels of Figures 1–4.

3.2. Initial Selection of Broad $H\alpha$ Candidates

Once we obtained continuum-subtracted spectra, we used, as a first pass, a simple algorithm to cull objects with excess emission in the region 6300–6700 Å that is potentially broad $H\alpha$ emission. We began by removing any narrow emission lines from this spectral region by adaptively smoothing it, iteratively removing outlier points. We then calculated the mean rms normalized to the dispersion in a line-free spectral region (5600–6000 Å), and integrated flux of the region. Since the spectra are continuum-subtracted, any object with a non-zero mean, rms, or integrated flux is a candidate for having broad $H\alpha$ emission. By trial and error we chose thresholds in the mean, integrated flux and normalized rms that identified all broad-line objects down to a very low contrast. We conservatively chose a low threshold, which increased our contamination rate but enhanced our completeness. The resulting sample from this procedure comprised 4163 candidates. As an initial cut, this technique has the benefit of being computationally inexpensive (important for an initial sample as large as the DR1). It has two major disadvantages: potential incompleteness and high contamination. Contaminants included misclassified late-type stars, which tend to have a broad maximum near 6500 Å that can be mistaken for broad $H\alpha$ emission (Ho et al. 1997c), and objects of unknown origin with large calibration errors or whose spectra have been corrupted in the $H\alpha$ region. We experimented with using pipeline flags to automatically remove these but in the end flagged them by hand. A more significant contaminant comes from incomplete removal of narrow emission lines from starburst galaxies with extremely strong line emission, or emission-line galaxies with multicomponent, relatively broad narrow lines. Detailed profile fitting, as described below, is required to isolate galaxies with a truly kinematically distinct broad-line component.

3.3. Emission-Line Profile Fitting

The broad $H\alpha$ feature, a reliable signature of AGN activity (see Ho et al. 1997c), is coincident with a combination of

narrow $H\alpha$ emission and the flanking [N II] $\lambda\lambda 6548, 6583$ doublet. While in many cases the broad-line emission in our candidates is evident by eye, the $H\alpha$ + [N II] region is sufficiently complicated that some care is needed to determine the presence or absence of a broad $H\alpha$ component. In addition to imperfect removal of starlight, the shape of the narrow lines themselves may confuse the detection of broad $H\alpha$. There are often broad, non-Gaussian wings, multiple peaks, and asymmetries in the narrow lines that can mimic or hide a true broad component to $H\alpha$. We therefore use a profile-fitting procedure, similar to that of Ho et al. (1997c), to model the narrow components based on regions of the spectrum less prone to blending and confusion. We can then determine objectively whether a broad component is present.

While the profiles of the narrow emission lines in some AGNs are known to vary as a function of critical density and ionization parameter (e.g., Pelat et al. 1981; Filippenko & Halpern 1984; Filippenko 1985; De Robertis & Osterbrock 1986), empirically the line profile of [S II] $\lambda\lambda 6716, 6731$ is generally well matched to those of [N II] and narrow $H\alpha$ (Filippenko & Sargent 1988; Ho et al. 1997c). Therefore, we model the [S II] doublet with a superposition of Gaussian components and then scale this model to fit the $H\alpha$ + [N II] narrow lines. We use up to four Gaussian components when it is statistically justified. We do not ascribe any particular physical significance to the individual components, but they allow us to describe the line shape as fully as the data quality allows. The two [S II] lines are assumed to have the same profile and are fixed in separation by their laboratory wavelengths; the relative strengths of the two lines change with density and thus are allowed to vary in the fit. In a few cases in which [S II] is undetectable or too weak to yield a reliable fit, we construct a model using [O III] $\lambda 5007$. [O III] is both strong and nearly ubiquitous and may seem like a better choice for template fitting. Unlike [S II], the [O III] profile does not typically match that of [N II] in detail. [O III] often has a broad, blue shoulder to its profile, suggestive of an outflow origin (De Robertis & Osterbrock 1984, 1986; Whittle 1985). Nonetheless, [O III] still seems to be an acceptable substitute for [S II] when the latter is unavailable.

Once a satisfactory narrow-line model is achieved, it serves as a template for fitting the $H\alpha$ + [N II] complex. The centroids of each component are fixed relative to each other at their laboratory separations, and the relative strength of [N II] $\lambda 6583$ and [N II] $\lambda 6548$ is fixed at the theoretical value of 2.96. An additional broad component for $H\alpha$ is added if statistically warranted; we use as many Gaussians as needed, but generally no more than 2–3, to fully describe the complex shapes of some of the broad components. Our fits are shown as dotted lines in the right panels of Figures 1–4. From the final model for the broad $H\alpha$ line, we measure the FWHM of the profile and its integrated flux. This step eliminates a large number of broad $H\alpha$ candidates, leaving a sample of ~ 3200 genuinely broad-line objects.

3.4. Nonstellar Continuum Luminosity

As discussed below, in order to estimate BH masses, we need to know the luminosity of the featureless nonstellar (AGN) continuum, $L_{5100} \equiv \lambda L_\lambda$ at $\lambda = 5100$ Å. We obtain L_{5100} in two ways. For objects whose AGN component clearly dominates (e.g., objects 1, 5, and 6 in Fig. 1), we directly fit a single power law to the spectrum using spectral regions known to be relatively unaffected by strong emission lines, especially from Fe II, which is pervasive in AGN spectra and

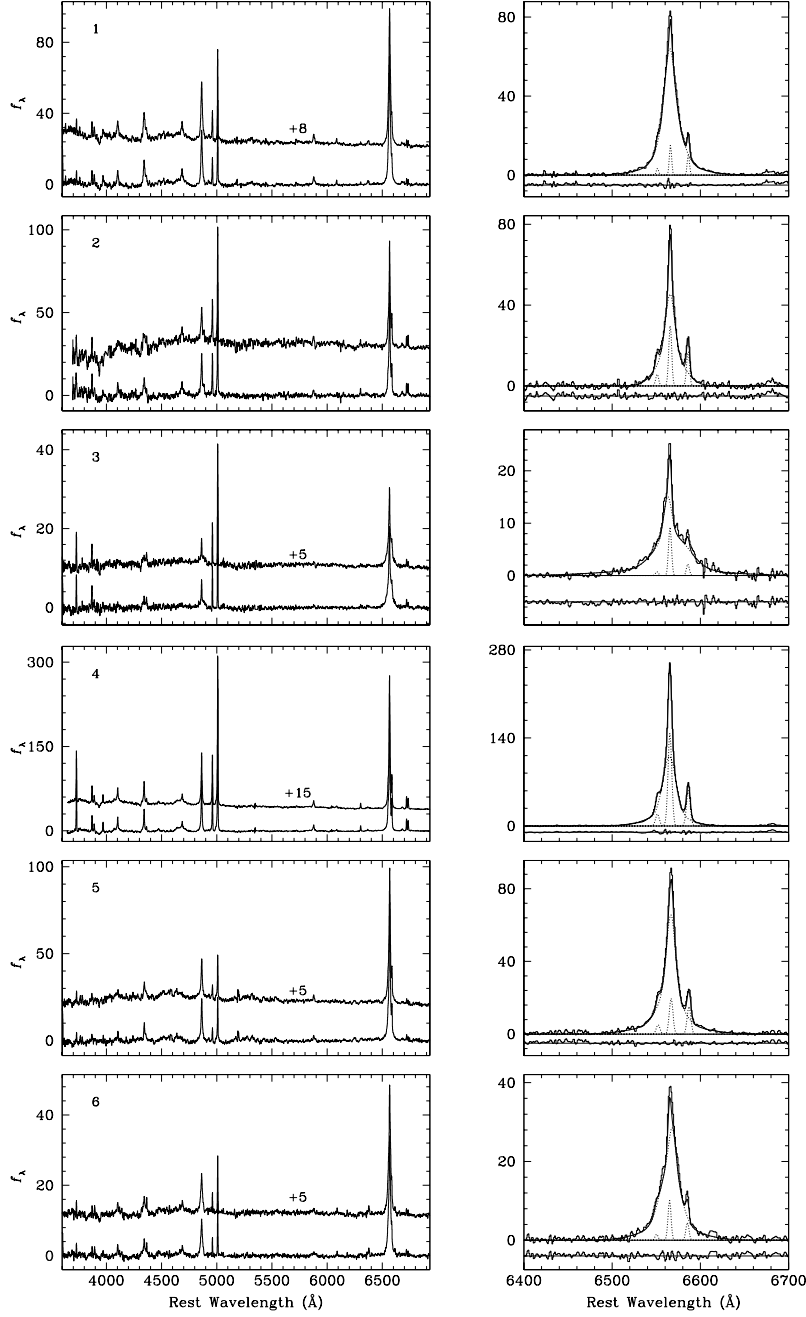


FIG. 1.—*Left:* Spectrum with (*bottom*) and without (*top*) starlight and continuum subtraction. For clarity, the top spectrum in some cases is offset by an additive constant, which is indicated. The top left corner of each panel gives the object identification number, which can be referenced in Table 1. *Right:* Enlargement of the region around $H\alpha + [N\ II] \lambda\lambda 6548, 6583$. In the upper plot, the data are shown in histogram, the individual models for the narrow and broad lines are shown in dotted lines, and the sum of all the fitted components is shown as a solid line. The lower plot gives the residuals of the fit. The ordinate of the plots are in units of 10^{-17} ergs $s^{-1} \text{ cm}^{-2} \text{ \AA}^{-1}$.

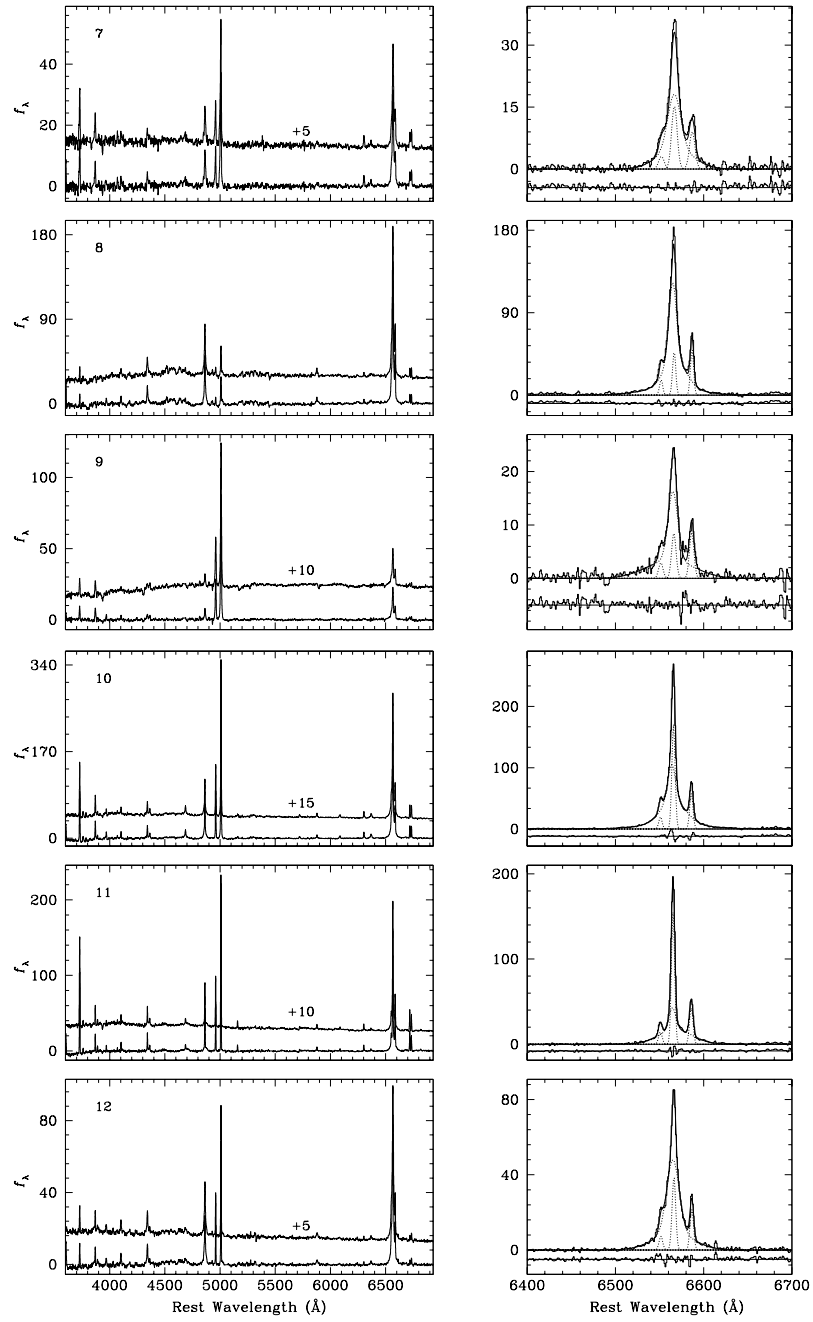


FIG. 2.—Same as Fig. 1, but for objects 7–12.

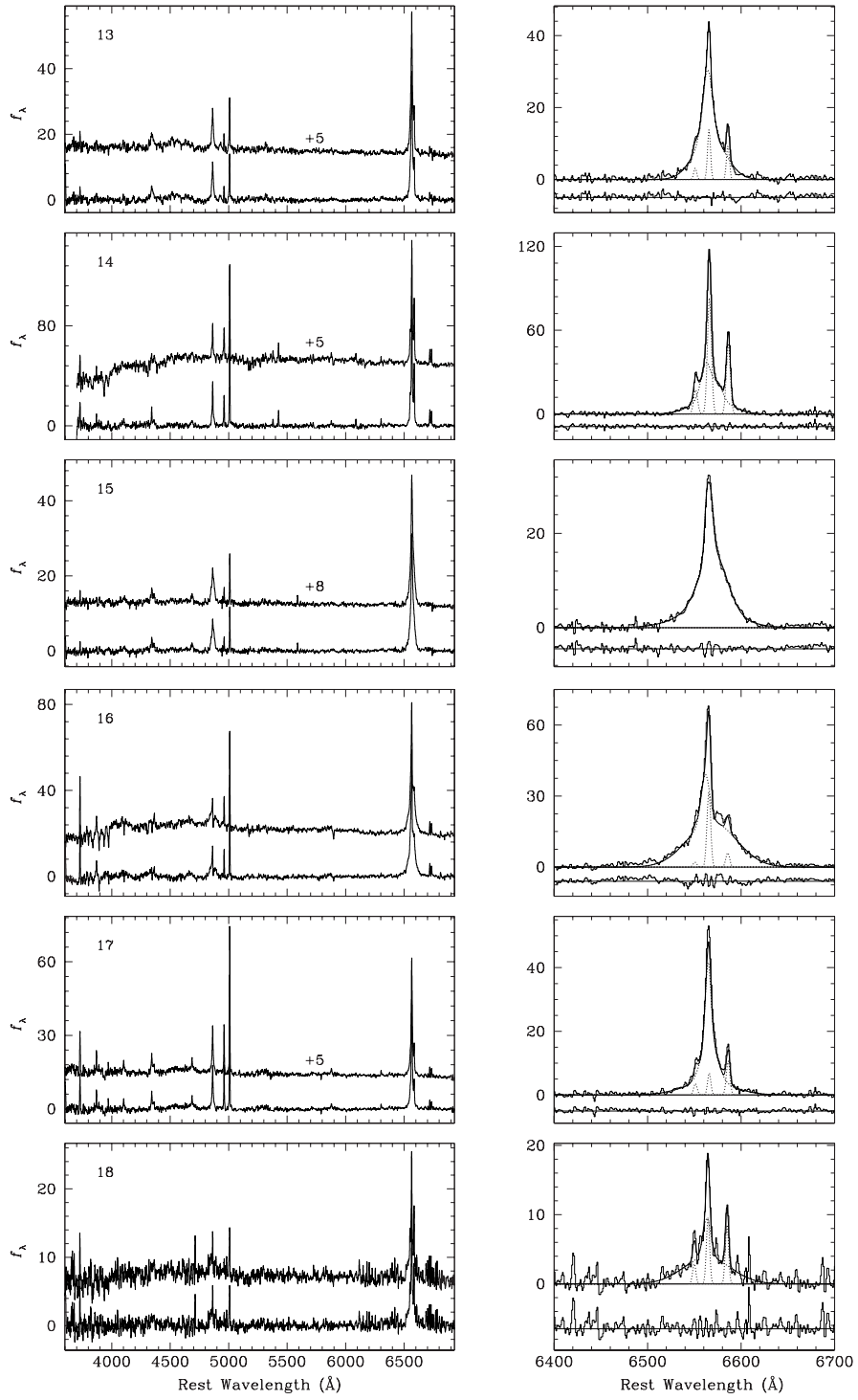


FIG. 3.—Same as Fig. 1, but for objects 13–18.

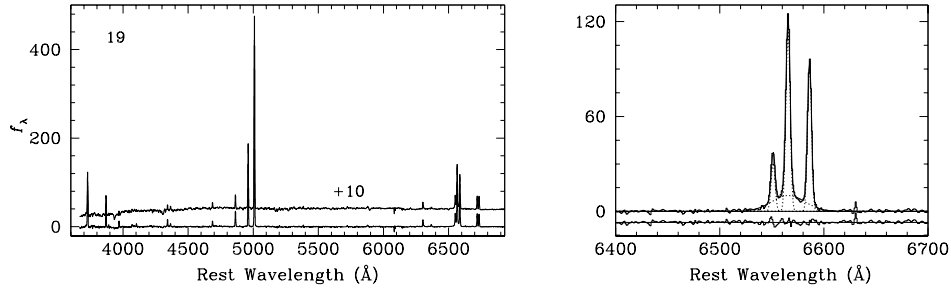


FIG. 4.—Same as Fig. 1, but for object 19.

can often be mistaken for continuum emission. The “continuum” windows we chose, guided by Francis et al. (1991), are 3700–3715, 3740–3800, 4041–4043, 4150–4250, 5550–5850, 6000–6290, and 6400–6450 Å. From the power-law fit we derive a slope and the continuum flux at 5100 Å.

For spectra with noticeable galaxy contribution, we must rely on the PCA decomposition to model the power-law contribution. From extensive experimentation with the PCA fits, we find that we can reliably recover the power-law component in objects where the AGN contribution at 5100 Å is $\geq 20\%$. In this study we only consider objects whose L_{5100} exceeds this threshold.

Once we have a measurement of the AGN power-law continuum, we can translate it into an equivalent g -band absolute magnitude, $M_g(\text{AGN})$, by convolving the power law with the response function of the SDSS g filter. In turn, we can estimate the g -band absolute magnitude of the host galaxy, $M_g(\text{host})$, by subtracting the AGN contribution to the total observed g -band luminosity.

3.5. Black Hole Masses

We estimate BH virial masses using a variant of the line width–luminosity mass scaling relation discussed by Kaspi et al. (2000). If the broad-line region (BLR) is in virial equilibrium, then the mass of the central BH is $M_{\text{BH}} \approx v^2 R_{\text{BLR}} / G$, where $v = (\sqrt{3}/2)v_{\text{FWHM}}$ and v_{FWHM} is the FWHM of the broad component of $\text{H}\beta$, R_{BLR} is the radius of the BLR, and G is the gravitational constant. For a sample of 34 low-redshift type 1 AGNs studied with reverberation mapping, Kaspi et al. (2000) found an empirical relation between the continuum luminosity of the AGN at 5100 Å and the size of the BLR:

$$R_{\text{BLR}} = 32.9_{-1.9}^{+2.0} \left(\frac{L_{5100}}{10^{44} \text{ ergs s}^{-1}} \right)^{0.700 \pm 0.033} \text{ lt-days}. \quad (1)$$

With this scaling relation, the virial mass is simply

$$M_{\text{BH}} = 4.82 \times 10^6 \left(\frac{L_{5100}}{10^{44} \text{ ergs s}^{-1}} \right)^{0.7} \left(\frac{v_{\text{FWHM}}}{1000 \text{ km s}^{-1}} \right)^2 M_{\odot}. \quad (2)$$

While it is conventional to use $\text{H}\beta$ to determine v_{FWHM} , we have decided to use $\text{H}\alpha$ as a surrogate instead. $\text{H}\alpha$ is at least a factor of 3 stronger than $\text{H}\beta$ and therefore much easier to measure for low-luminosity sources or in objects where host galaxy contamination is severe. Another advantage of $\text{H}\alpha$ is that, despite blending with $[\text{N II}]$ emission, it is still much easier to measure because it is not strongly affected by nearby

Fe II emission, as is the case for $\text{H}\beta$ (see, e.g., Francis et al. 1991).

The currently popular formalism to derive virial BH masses for broad-line AGNs is calibrated against the sample of AGNs with reverberation mapping data (Kaspi et al. 2000). As discussed by Krolik (2001), this simplistic approach may be subject to a variety of unquantified systematic uncertainties. Nevertheless, Gebhardt et al. (2000b) and Ferrarese et al. (2001) have demonstrated, for a subset of the reverberation-mapped AGNs with available stellar velocity dispersions, that the virial BH masses, remarkably if unexpectedly, do roughly conform to the $M_{\text{BH}}\text{-}\sigma_*$ relation of inactive galaxies. Interestingly, both NGC 4395 and POX 52 follow the low-mass extrapolation of the Tremaine et al. (2002) fit to the $M_{\text{BH}}\text{-}\sigma_*$ relation (Filippenko & Ho 2003; Barth et al. 2004; Ho 2004b). The virial masses scatter around the $M_{\text{BH}}\text{-}\sigma_*$ relation with a spread of ~ 0.5 dex, which for the moment can be taken as an estimate of the systematic uncertainty of this method.

Certain aspects of our analysis may introduce additional errors into the mass measurements, although we believe that they are small relative, or at most comparable, to the intrinsic systematic uncertainty discussed above. There are two basic measurements that affect our mass determinations, namely, L_{5100} and v_{FWHM} . Both of these quantities become increasingly challenging to measure when galaxy contamination is large. The complete profile of weak emission lines with very broad wings becomes very difficult to measure when the contrast between the AGN and the galaxy is low. Dilution from host galaxy starlight, which can never be removed perfectly, *always* leads one to underestimate the true width of a weak, low-contrast broad emission line. This has been demonstrated most conclusively for some objects by comparing starlight-subtracted ground-based spectra with small-aperture spectra taken with the *Hubble Space Telescope* (e.g., Ho et al. 2000; Shields et al. 2000); the small-aperture spectra, largely free from starlight contamination, reveal *much* broader $\text{H}\alpha$ wings than the ground-based spectra. To mitigate this problem, and that associated with measuring L_{5100} (§ 3.4), in this study we have chosen to concentrate on objects in which the AGN component is largely dominant. This is evident from Figures 1 to 4 by the overall weakness of stellar absorption features in the spectra.

We note that substituting $\text{H}\alpha$ for $\text{H}\beta$ to measure v_{FWHM} should introduce negligible additional uncertainty into the mass estimates. Although the physical conditions in the BLR that give rise to $\text{H}\alpha$ and $\text{H}\beta$ emission in principle may be slightly different (e.g., Kwan & Krolik 1981), in practice the two lines are observed to have rather similar velocity profiles, with $\text{H}\beta$ on average being only slightly broader than $\text{H}\alpha$. From a study of 19 Seyfert 1 galaxies, Osterbrock & Shuder (1982) find that the broad $\text{H}\beta$ and $\text{H}\alpha$ lines have nearly identical full widths at zero intensity, and on average $\text{H}\beta$ is

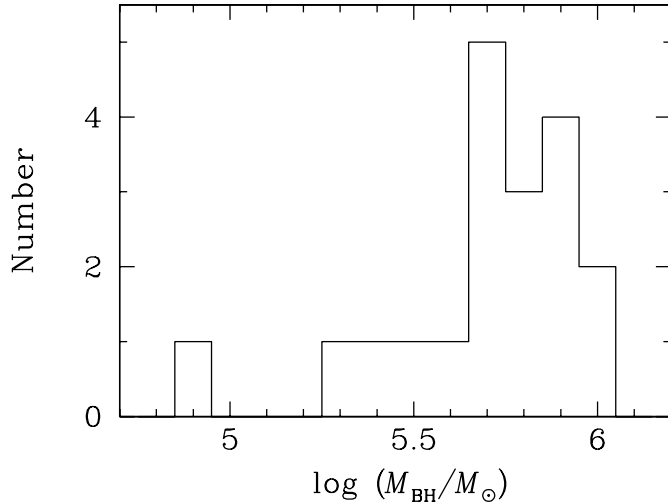


FIG. 5.—Distribution of virial BH masses for our sample.

16% broader than $H\alpha$ at FWHM. If this trend holds, then we may be underestimating the mass in equation (2) by $\sim 30\%$, which is insignificant compared to the much larger 0.5 dex uncertainty in the virial mass zeropoint. Moreover, in the two AGNs with intermediate-mass BHs known to date—NGC 4395 and POX 52—there is no indication that the line profile of broad $H\alpha$ differs systematically from that of $H\beta$ (Filippenko & Sargent 1989; Kraemer et al. 1999; Barth et al. 2004). We await future measurements of stellar velocity dispersions to investigate potential systematic differences in our virial mass estimates, but for now we assume that the $H\alpha$ line width can be substituted for that of $H\beta$.

With the BH virial masses at hand, we are in a position to select the intermediate-mass BH candidates. With a cut-off of $10^6 M_{\odot}$, the final sample contains 19 broad-line objects (Fig. 5). Their spectra are in Figures 1–4. Table 1 shows the

basic properties of the sample, Table 2 lists measurements of the emission-line parameters, and Table 3 gives the luminosity and mass estimates.

4. DISCUSSION

We employ a simple technique to exploit the breadth of the SDSS galaxy spectroscopy to extend the demography of central BHs at least 1 order of magnitude below the $10^6 M_{\odot}$ threshold, a regime hardly explored previously. We present the first sizable sample of AGNs with candidate intermediate-mass BHs. The sample contains 19 objects with virial BH masses in the range $M_{\text{BH}} \approx 8 \times (10^4 - 10^6) M_{\odot}$ (Fig. 5). We now briefly examine some of the properties of these objects.

4.1. Spectral Properties

In the literature to date, the closest analog to our sample (aside from NGC 4395 and POX 52) is the class of AGNs known as narrow-line Seyfert 1 galaxies (NLS1s), which are thought to possess relatively low-mass BHs emitting at a high fraction of their Eddington rates (e.g., Boroson 2002). Since our sample selection required a relatively prominent AGN component relative to the host galaxy, the sample should preferentially single out AGNs in a relatively “high” state.

First classified as a group by Osterbrock & Pogge (1985), NLS1s are typically characterized by broad permitted lines with $\text{FWHM} \lesssim 2000 \text{ km s}^{-1}$, prominent Fe II emission, and relatively weak [O III] $\lambda\lambda 4959, 5007$ lines. NLS1s also tend to emit copiously in the soft X-ray band (e.g., Boller et al. 1996; but see Williams et al. 2002), presumably as a consequence of their high accretion rates (Pounds et al. 1995). Our sample conforms to some, but not all, of these expectations. By the line width criterion, certainly all of the objects would technically qualify as “narrow-line” sources: the broad $H\alpha$ component has FWHM ranging from 464 to 1730 km s^{-1} , with an average value of 836 km s^{-1} . However, we note that our sample shows a greater diversity of Fe II and [O III]

TABLE 1
THE SDSS SAMPLE

ID (1)	SDSS Name (2)	z (3)	g (4)	$g - r$ (5)	A_g (6)
1.....	SDSS J010712.03+140844.9	0.0768	18.49	0.62	0.26
2.....	SDSS J024912.86–081525.6	0.0295	16.55	0.66	0.11
3.....	SDSS J032515.59+003408.4	0.102	19.51	0.70	0.49
4.....	SDSS J082912.67+500652.3	0.0434	17.68	0.41	0.16
5.....	SDSS J094310.12+604559.1	0.0742	18.32	0.57	0.09
6.....	SDSS J101108.40+002908.7	0.100	19.39	0.56	0.13
7.....	SDSS J101627.32–000714.5	0.0943	19.31	0.66	0.13
8.....	SDSS J114008.71+030711.4	0.0811	17.32	0.51	0.07
9.....	SDSS J115138.24+004946.4	0.194	19.02	1.20	0.10
10.....	SDSS J124035.81–002919.4	0.0809	18.00	0.47	0.09
11.....	SDSS J125055.28–015556.6	0.0814	18.23	0.37	0.08
12.....	SDSS J135724.52+652505.8	0.106	18.45	0.36	0.07
13.....	SDSS J141234.67–003500.0	0.126	18.19	0.59	0.17
14.....	SDSS J143450.62+033842.5	0.0281	15.60	0.62	0.14
15.....	SDSS J144507.30+593649.9	0.127	19.98	0.41	0.03
16.....	SDSS J170246.09+602818.9	0.0690	18.22	0.59	0.07
17.....	SDSS J172759.15+542147.0	0.0994	19.27	0.57	0.14
18.....	SDSS J232159.06+000738.8	0.183	19.39	0.71	0.16
19.....	SDSS J233837.10–002810.3	0.0355	16.87	0.60	0.11

NOTE.—Col. (1): Identification number assigned in this paper. Col. (2): Official SDSS name. Col. (3): Redshift measured by the SDSS pipeline. Col. (4): Petrosian g -magnitude. Col. (5): Petrosian $g - r$ color. Col. (6): Galactic extinction in the g band.

TABLE 2
EMISSION-LINE MEASUREMENTS

ID (1)	[O II] λ 3727 (2)	Fe II λ 4570 (3)	(H β) _n (4)	(H β) _b (5)	[O III] λ 5007 (6)	[O I] λ 6300 (7)	(H α) _n (8)	(H α) _b (9)	[N II] λ 6583 (10)	[S II] λ 6716 (11)	[S II] λ 6731 (12)	FWHM _{Hα} (km s ⁻¹) (13)	FWHM _[O III] (km s ⁻¹) (14)
1.....	0.154	1.59	0.046	1.48	362.0	0.021	0.143	4.73	0.098	0.043	0.043	830	260
2.....	0.273	<1.04	0.079	0.88	519.0	0.053	0.245	1.95	0.141	0.077	0.074	732	262
3.....	0.225	1.07	0.070	0.73	192.0	<0.002	0.217	3.25	0.051	0.064	0.038	916	199
4.....	0.307	0.26	0.139	0.42	1880.0	0.030	0.431	1.48	0.165	0.073	0.063	870	238
5.....	0.081	4.29	0.167	1.79	210.0	<0.005	0.517	7.98	0.400	0.097	0.055	698	291
6.....	0.171	2.83	0.074	1.93	104.0	<0.008	0.461	8.31	0.206	0.099	0.067	919	261
7.....	0.309	0.55	0.093	0.25	453.0	0.081	0.288	1.16	0.170	0.090	0.095	940	449
8.....	0.096	6.98	0.311	1.89	241.0	0.182	0.966	11.0	1.00	0.242	0.241	591	297
9.....	0.085	<0.55	0.019	0.07	1050.0	<0.001	0.060	0.46	0.062	0.014	0.017	703	504
10.....	0.240	0.41	0.127	0.25	2150.0	0.048	0.396	1.35	0.138	0.071	0.069	722	255
11.....	0.578	0.44	0.219	0.20	1140.0	0.043	0.680	1.01	0.203	0.155	0.118	642	212
12.....	0.133	0.92	0.154	0.75	463.0	0.020	0.478	2.87	0.263	0.040	0.054	872	231
13.....	0.191	3.55	0.157	1.58	126.0	<0.007	0.487	6.65	0.335	0.114	0.074	785	275
14.....	0.219	<1.07	0.273	0.52	541.0	0.053	0.848	1.96	0.523	0.159	0.140	1089	276
15.....	0.079	2.12	0.012	2.93	83.4	<0.004	<0.038	11.8	<0.038	<0.061	<0.061	750	219
16.....	0.565	<1.53	0.211	1.18	257.0	0.028	0.654	6.17	0.124	0.148	0.115	919	234
17.....	0.244	0.97	0.028	0.65	386.0	0.033	0.086	2.08	0.146	0.059	0.051	464	233
18.....	0.707	<7.30	0.325	0.75	49.5	<0.038	1.01	7.24	0.899	<0.434	<0.434	707	342
19.....	0.234	<0.13	0.075	...	2550.0	0.045	0.232	0.16	0.175	0.072	0.069	1730	216

NOTES.—Col. (1): Identification number assigned in this paper. Col. (2)–(12): All fluxes are relative to that of [O III] λ 5007, which is listed in units of 10^{-17} ergs s⁻¹ cm⁻². Note that these are observed values; no extinction correction has been applied. The subscripts *n* and *b* in cols. (4)–(5) and (8)–(9) refer to the narrow and broad components of the line, respectively. The narrow component of H β is sufficiently weak that it was impossible to obtain a robust measurement of its strength, so we fixed it to that of the narrow H α component, assuming an intrinsic ratio of H α /H β = 3.1 for AGNs (Halpern & Steiner 1983; Gaskell & Ferland 1984). Col. (13)–(14): These are the observed line widths; they have not been corrected for instrumental resolution. The FWHM_{H α} was derived from the model fit to the broad H α line, as described in § 3.3.

TABLE 3
LUMINOSITY AND MASS MEASUREMENTS

ID (1)	$M_g(\text{total})$ (2)	$M_g(\text{AGN})$ (3)	$M_g(\text{host})$ (4)	β (5)	$\log L_{5100}$ (6)	$\log M_{\text{BH}}$ (7)	$\log L_{\text{bol}}/L_{\text{Edd}}$ (8)
1.....	-19.1	-17.8	-18.7	0.60	43.06	5.86	0.092
2.....	-18.9	-15.4	-18.9	1.00	41.87	4.92	-0.15
3.....	-18.7	-17.4	-18.4	0.11	42.91	5.84	-0.03
4.....	-18.6	-17.1	-18.3	0.88	42.80	5.72	-0.02
5.....	-19.2	-17.7	-18.9	0.27	43.10	5.74	0.254
6.....	-18.8	-17.7	-18.3	0.076	42.93	5.86	-0.03
7.....	-18.8	-17.1	-18.5	0.44	42.97	5.91	-0.04
8.....	-20.4	-18.3	-20.2	0.14	43.35	5.77	0.475
9.....	-20.8	-18.4	-20.6	1.00	43.02	5.69	0.223
10.....	-19.7	-18.4	-19.4	0.46	43.33	5.93	0.296
11.....	-19.5	-17.5	-19.3	0.76	43.22	5.75	0.362
12.....	-19.9	-18.1	-19.7	0.79	43.17	5.98	0.082
13.....	-20.6	-18.1	-20.5	0.39	43.32	5.99	0.218
14.....	-19.7	-15.4	-19.7	1.00	41.92	5.30	-0.48
15.....	-18.8	-18.3	-17.8	0.24	42.97	5.71	0.153
16.....	-19.1	-17.4	-18.9	1.00	42.53	5.58	-0.15
17.....	-18.9	-17.6	-18.5	0.31	43.05	5.35	0.592
18.....	-20.3	-18.0	-20.1	1.00	43.09	5.74	0.240
19.....	-19.0	-15.0	-19.0	1.00	41.69	5.54	-0.95

NOTES.—Col. (1): Identification number assigned in this paper. Col. (2): Total g -band absolute magnitude. Col. (3): AGN g -band absolute magnitude, estimated from L_{5100} given in col. (6) and a conversion from L_{5100} to M_g assuming $f_{\lambda} \propto \lambda^{-\beta}$, where β is given in col. (5); typical uncertainty is ~ 0.4 mag. Col. (4): Host galaxy g -band absolute magnitude, obtained by subtracting the AGN luminosity from the total luminosity. Col. (5): Power-law slope β , where $f_{\lambda} \propto \lambda^{-\beta}$; typical uncertainty is $\sim 10\%$. A value of 1.00 indicates that it was fixed in the PCA decomposition. Col. (6): AGN continuum luminosity at 5100 Å (ergs s⁻¹), estimated from a power-law fit to the continuum; typical uncertainty is $\sim 10\%$. Col. (7): Virial mass estimate of the BH (M_{\odot}). Col. (8): Ratio of the bolometric luminosity (see text) to the Eddington luminosity.

strengths than in previous samples of NLS1s. Fe II emission is common but not ubiquitous.¹ For example, the intensity ratio of Fe II $\lambda 4570$ relative to total (broad+narrow) H β , where Fe II $\lambda 4570$ is the complex between 4434 and 4680 Å, varies from ~ 0.465 to 3.17, with a mean of 1.32 ± 0.16 , calculated using the Kaplan-Meier product-limit estimator to account for upper limits (Feigelson & Nelson 1985). This is to be compared with $\langle \text{Fe}\lambda 4570/\text{H}\beta(\text{total}) \rangle = 0.67 \pm 0.04$ for the 56 NLS1s presented by Véron-Cetty et al. (2001). Similarly, in our sample $[\text{OIII}]/\text{H}\beta(\text{total}) = 0.335\text{--}12.0$, with a mean of 2.24 ± 0.72 . In contrast Véron-Cetty et al. (2001) find $\langle [\text{OIII}]/\text{H}\beta(\text{total}) \rangle = 0.65 \pm 0.09$, and Constantin & Shields 2003 find $\langle [\text{OIII}]/\text{H}\beta(\text{total}) \rangle = 0.39$ for their composite spectrum of 22 NLS1s. Thus, compared to classical NLS1s, we find stronger [O III] and Fe II emission. The distribution of power-law slopes for the AGN-dominated spectra are also quite interesting (Table 3). While $1.5 < \beta < 1$ is a standard range for luminous AGNs (e.g., Malkan 1988), we find an average value of $\beta = 0.42$.

Only six of the 19 sources (30%) were detected in the *ROSAT* All-Sky Survey (Table 4), confirming the finding of Williams et al. (2002) that not all NLS1s have detectable soft X-ray (0.5–2 keV) emission. The data are not of sufficiently high quality to make spectral analysis possible, so to convert count rate to flux we assume a power-law spectrum with a fixed photon index of $\Gamma = 3$, which is roughly the average value observed in previous *ROSAT* studies of NLS1s (e.g., Boller et al. 1996; Véron-Cetty et al. 2001; Williams et al.

2002). We use the online program webPIMMS² to do the conversion, assuming that the only source of absorption is due to the Galaxy along the line of sight. The derived soft X-ray luminosities range from $\sim 10^{42.1}$ to $10^{42.9}$ ergs s⁻¹ (Table 4), which probably can be attributed mostly to the AGN. The host galaxies of our sample are relatively faint (§ 4.3), with absolute g -band magnitudes that roughly translate to $L_B \approx 10^{9.4}\text{--}10^{10.1} L_{\odot}$ (Fukugita et al. 1996). If these galaxies follow the $L_B\text{--}L_X$ relation of normal galaxies (e.g., Fabbiano 1989), they are expected to have $L_X \approx 10^{38.5}$ ergs s⁻¹.

Only one of the objects was detected in the Very Large Array³ FIRST survey (Becker et al. 1995), although the entire

² See <http://heasarc.gsfc.nasa.gov/Tools/w3pimms.html>.

³ The VLA is operated by the National Radio Astronomy Observatory, which is a facility of the National Science Foundation, operated under cooperative agreement by Associated Universities, Inc.

TABLE 4
X-RAY DETECTIONS

ID (1)	C (2)	$\log N_{\text{H}}$ (3)	$\log f_X$ (4)	$\log L_X$ (5)
1.....	0.0483	20.59	-12.21	42.92
7.....	0.0276	20.59	-12.46	42.86
8.....	0.113	20.37	-12.86	42.32
12.....	0.100	20.30	-12.92	42.51
14.....	0.0564	20.40	-12.16	42.07
17.....	0.0174	20.50	-12.66	42.70

NOTES.—Col. (1): Identification number assigned in this paper. Col. (2): *ROSAT* count rate (counts s⁻¹). Col. (3): Galactic column N_{H} (cm⁻²), calculated following Dickey & Lockman (1990). Col. (4): X-ray flux in the 0.5–2 keV band (ergs s⁻¹ cm⁻²) assuming a power-law spectrum with $\Gamma = 3$ and N_{H} from col. (3). Col. (5): X-ray luminosity in the 0.5–2 keV band (ergs s⁻¹).

¹ The same comment applies to NGC 4395 and POX 52, both of which may be formally regarded as NLS1s. Fe II multiplets can be seen in the UV spectrum of NGC 4395 (Filippenko et al. 1993), but they are quite weak in its optical spectrum (Filippenko & Sargent 1989). Fe II emission is also not prominent in the optical spectrum of POX 52 (Barth et al. 2004).

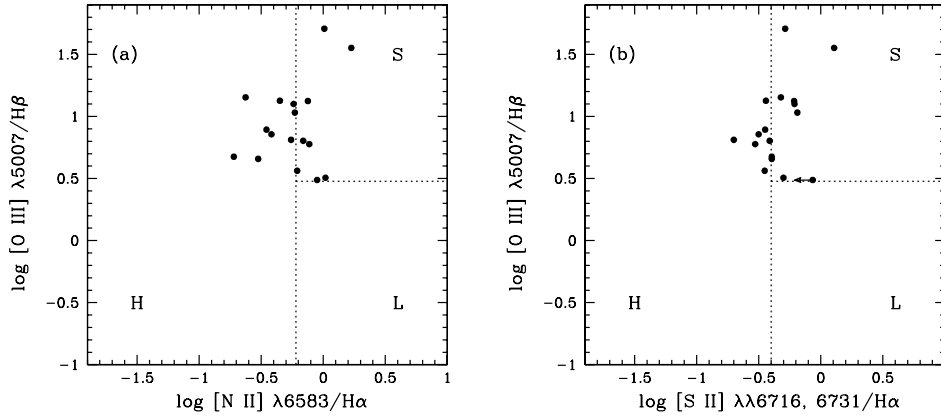


Fig. 6.—Diagnostic diagram plotting $\log [O\text{ III}] \lambda 5007/H\beta$ vs. (a) $\log [N\text{ II}] \lambda 6583/H\alpha$ and (b) $\log [S\text{ II}] \lambda\lambda 6716, 6731/H\alpha$. The line ratios have not been corrected for reddening, but this should not matter because of the close wavelength separation of the lines. Object 15 was omitted because $[N\text{ II}]$, $[S\text{ II}]$, and narrow $H\alpha$ were not detected. The dotted lines mark the boundaries of the three main classes of emission-line nuclei, according to the convention of Ho et al. (1997a): “H” = $H\text{ II}$ nuclei, “S” = Seyferts, and “L” = LINERs.

sample overlapped with the FIRST survey area. Object 10 has a 20 cm flux density of 1.3 mJy, which corresponds to a spectral power of 2.0×10^{22} W Hz $^{-1}$. This level of radio emission is not atypical of normal galaxies (Condon 1992), so we cannot conclude, without additional evidence, that it is associated with AGN activity.

Figure 6 places the sources on two commonly used line intensity ratio diagnostic diagrams. The dotted lines schematically denote the boundaries used by Ho et al. (1997a) to demarcate the main classes of emission-line objects. Although all the objects are clearly AGNs by the presence of their prominent broad lines, some of them in the $[O\text{ III}]/H\beta$ versus $[N\text{ II}]/H\alpha$ and $[O\text{ III}]/H\beta$ versus $[S\text{ II}]/H\alpha$ diagrams formally lie outside of the AGN zone ($[N\text{ II}]/H\alpha \geq 0.6$ and $[S\text{ II}]/H\alpha \geq 0.4$). This is rarely seen in local type 1 AGNs (Ho et al. 1997a). Since the SDSS fibers subtend a significant fraction of each galaxy, the narrow emission-line ratios of the nuclei are, at least in part, contaminated by host galaxy emission, which would have the effect of lowering the $[S\text{ II}]/H\alpha$ and $[N\text{ II}]/H\alpha$ ratios. Thus, one expects, a priori, that AGNs not selected by their narrow lines will, in some cases, exhibit narrow-line ratios that fall below the AGN threshold.

4.2. Nuclear Luminosities and Eddington Ratios

Since our sample was selected to have low BH mass, we expect that the AGNs will generally be of relatively low luminosity. Figure 7 shows the distribution of nuclear g -band absolute magnitudes for the sample. To estimate this quantity, we first compute L_{5100} (as described above), which is then transformed to M_g . For those spectra with direct power-law fits, we use the best-fit spectral index, while for the remainder we assume an $f_\lambda \propto \lambda^{-1}$ spectrum. The AGN component has absolute magnitudes ranging from $M_g \approx -15$ to -18 mag. Note that these nuclear luminosities, although generally not as low as many local Seyfert galaxies (Ho & Peng 2001), are still significantly lower than in many previously studied low-redshift type 1 AGNs (e.g., Köhler et al. 1997).

It is of interest to compare the nuclear luminosities with respect to the Eddington luminosities. The selection criteria—low BH mass and a prominent AGN spectrum—are expected to favor objects with high Eddington ratios. A major uncertainty in this exercise is that we do not have a robust estimate of the bolometric luminosity but only a measurement of the optical luminosity (L_{5100}). Since the spectral energy distri-

butions of AGNs are known to vary significantly with accretion rate (Pounds et al. 1995; Ho 1999), it is doubtful that a single bolometric correction is always applicable. Nonetheless, assuming $L_{\text{bol}} = 9.8L_{5100}$ (McLure & Dunlop 2004), the derived Eddington ratios mostly cluster around $L_{\text{bol}}/L_{\text{Edd}} \approx 1$ (Fig. 8; Table 3), as expected.

4.3. Properties of the Host Galaxies

The morphology of the host galaxies of intermediate-mass BHs is of fundamental importance for understanding the origin of this class of objects and their relationship to the overall demography of central BHs in galaxies. The two currently known nuclear intermediate-mass BHs are found in anomalous hosts compared to the local AGN population (Ho et al. 1997b; Ho 2003; Kauffmann et al. 2003), which is invariably affiliated with massive, bulge-containing galaxies. Similarly, essentially every galaxy known to contain a supermassive BH has a bulge. Yet, NGC 4395, which without a doubt lacks a bulge, evidently hosts a nuclear BH (Filippenko & Ho 2003). The same could be said of POX 52 (Ho 2004b). Although POX 52 appears to be a dwarf elliptical galaxy (Barth et al. 2004), this class of spheroids should be regarded as physically distinct from classical bulges (Bender et al. 1992), and they may have originated as tidally stripped late-type disk galaxies (e.g., Moore et al. 1996). Thus, both NGC 4395 and POX 52 provide compelling evidence that a classical bulge is *not* necessary for the formation of a central BH.

We have attempted to estimate the luminosities of the host galaxies by subtracting the contribution of the AGN from the total (Petrosian) g -band magnitude of the AGN plus host. As illustrated in Figure 7 (see also Table 3), in most cases the luminosities of the AGNs are sufficiently low that they hardly perturb the distribution of total magnitudes; thus, the host galaxy magnitudes should be quite robust. Interestingly, the hosts are relatively low luminosity and therefore more likely to be late-type galaxies: $M_g(\text{host})$ ranges from -17.8 to -20.6 mag, with an average value of -19.2 . According to Blanton et al. (2003), the luminosity function of galaxies at $z = 0.1$ has $M_g^* = -19.39 + 5 \log h$. For $h = 0.72$, as assumed here, $M_g^* = -20.1$ mag. Thus, the hosts of our sample are ~ 1 mag fainter than M_g^* .

Our selection technique is unbiased with respect to galaxy morphology. Unfortunately, we have very limited information on the morphological types of the host galaxies. The low

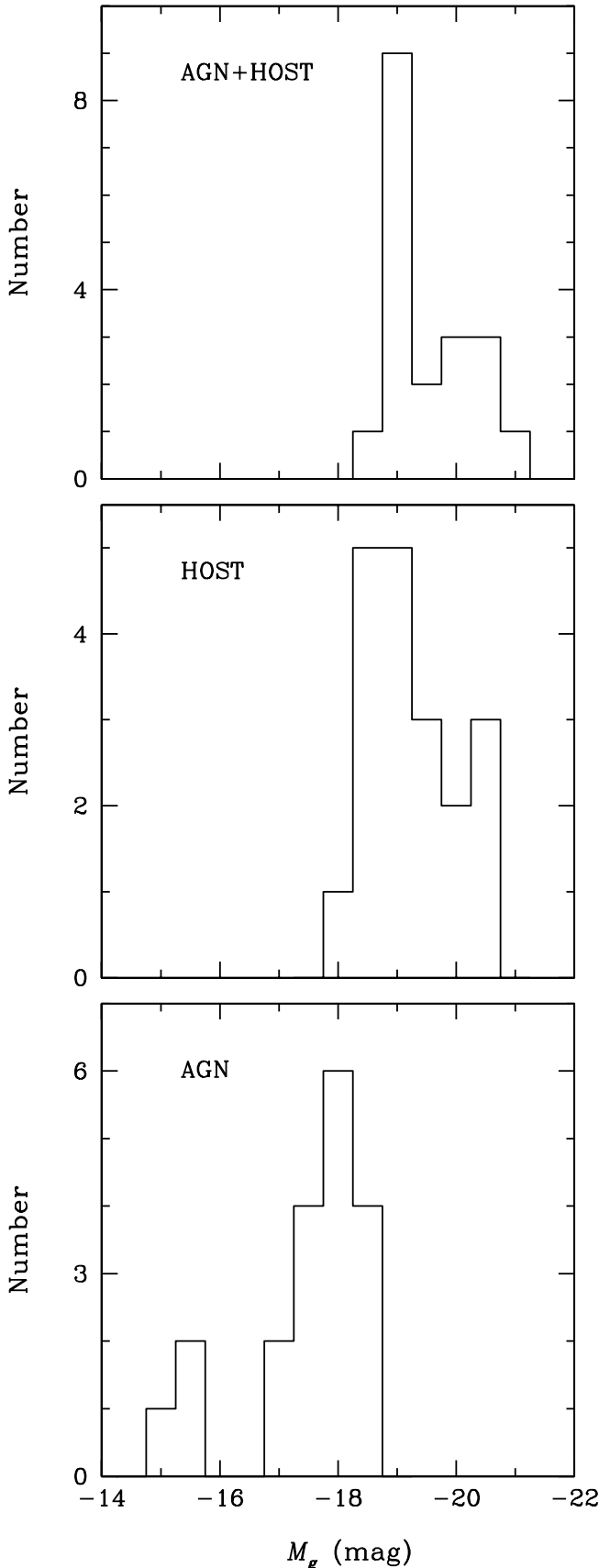


FIG. 7.—Distributions of g -band absolute magnitudes. The magnitudes pertain to the entire system (*top*), the host galaxy alone (*middle*), and the AGN alone (*bottom*). The AGN contribution was estimated from L_{5100} , which was then converted to a g -magnitude assuming an $f_\lambda \propto \lambda^{-\beta}$ spectrum, where β is shown in Table 3.

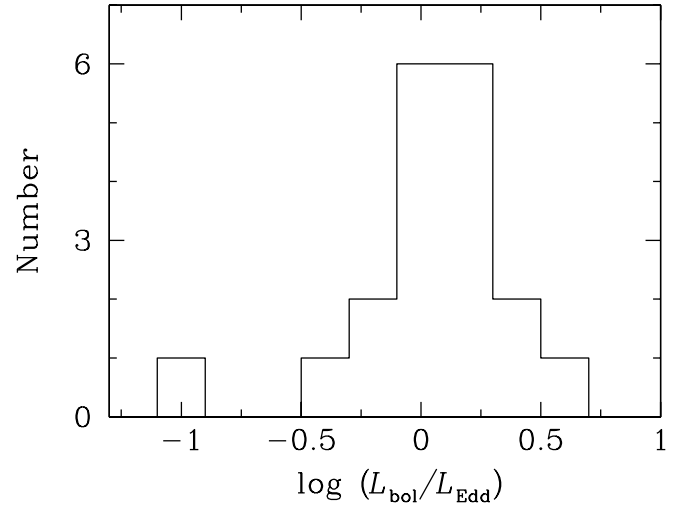


FIG. 8.—Distribution of Eddington ratios. The bolometric luminosity was estimated from L_{5100} (see text).

resolution of the SDSS imaging makes morphological classification difficult for these objects. By selection, the galaxy centers are dominated by an AGN core, which makes it impossible to say anything meaningful about the central structure of the galaxies. If the low BH masses are accompanied by a low-mass (low-luminosity) galaxy or bulge, this makes it doubly hard to detect. We show a selection of the more interesting images in Figure 9. Based on the SDSS imaging, one-third of the galaxies clearly have a disklike component. Of the six that show disks, five have significant galaxy light in their spectra, which required PCA decomposition. Given the low luminosities of these galaxies, perhaps they are analogs of NGC 4395. The remainder are barely resolved enough to tell, but could be consistent with compact spheroids. We caution that the images are of low resolution and sensitivity, so in many cases we may be insensitive to an extended stellar component. Higher resolution, deeper imaging, for example with the *Hubble Space Telescope*, is essential to determine the true morphology and detailed structural parameters of these hosts.

In lieu of resolved morphological information, the SDSS collaboration has developed statistical proxies that describe morphological trends (Shimasaku et al. 2001; Strateva et al. 2001). We consider the “eClass” (a PCA statistic), the $u-r$ color, and the “inverse concentration index.” The eClass ranges from -0.35 for early-type galaxies to $+0.5$ for late-type galaxies. The mean eClass of our sample is 0.24. This statistic is difficult to interpret because of the strong contamination by the AGN. For $\sim 150,000$ SDSS galaxies, Strateva et al. (2001) find a bimodal distribution in $u-r$ color, with the division at $u-r = 2.22$ mag, which roughly divides early and late types. Our galaxies have a mean color of $u-r \approx 1.51$, consistent with late-type galaxies. An inverse concentration index of ~ 0.3 corresponds to a de Vaucouleurs (1948) $r^{1/4}$ profile, while an exponential profile has an index of ~ 0.43 . The mean inverse concentration index of our objects is 0.41.

4.4. Implications and Future Work

While the discovery of the $M_{\text{BH}}-\sigma_*$ relation established a compelling link between the evolution of galaxies and central BHs, models of this process are faced with significant uncertainties. Possible models include seed BHs formed from

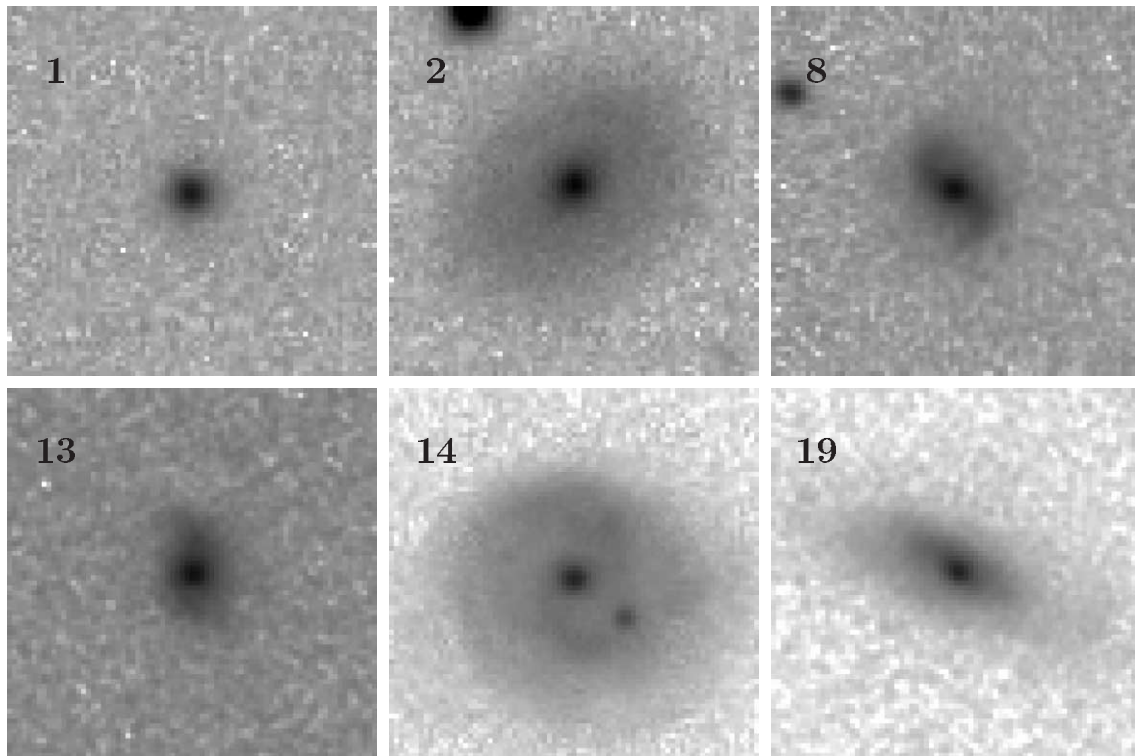


FIG. 9.—Sample SDSS g -band images of six objects. The vast majority of the sample are barely resolved and look similar to object 1. In all images north is up, and east is to the left. Each panel is $30'' \times 30''$.

Population III stars, which then gain mass through mergers (Schneider et al. 2002; Volonteri et al. 2003) or through accretion (Adams et al. 2001; Islam et al. 2003). Alternatively, seed BHs may form directly from a collapsing gas cloud (Koushiappas et al. 2004; for a more complete discussion, see the review by van der Marel 2004). However, there are few direct observational constraints on the nature of seed BHs, the path by which nuclear BHs grow, or the form of the BH mass function. The low end of the BH mass function, in particular, provides critical input to check theoretical models of quasar formation (e.g., Haehnelt et al. 1998; Bromley et al. 2004), and it affects predictions of future gravitational wave experiments such as the *Laser Interferometer Space Antenna* (Hughes 2002).

A useful approach, first proposed by Soltan (1982), matches the local BH mass density inferred from velocity dispersion measurements with an accretion history inferred from observations of luminous quasars. Yu & Tremaine (2002) conclude that, for standard assumptions about radiative efficiency and quasar lifetimes, accretion during the luminous quasar phase can account for the majority of the local BH mass density. Aside from the possibility of significant obscured accretion (Fabian 2004), this method is limited by its use of the SDSS velocity dispersion function, which at the moment is only well determined for early-type galaxies with $\sigma_* \gtrsim 200 \text{ km s}^{-1}$ (Sheth et al. 2003), corresponding to $M_{\text{BH}} \gtrsim 10^8 M_\odot$.

Much of the current observational and theoretical effort on intermediate-mass BHs has focused on studies of star clusters (Gebhardt et al. 2002; Gerssen et al. 2002) and so-called ultraluminous X-ray sources (see van der Marel 2004). The existence of BHs in either class of objects is still far from proven, and, in any event, their relationship to galactic nuclei is unclear. With the recognition that galaxies like NGC 4395 and POX 52 do harbor central intermediate-mass BHs, the

most straightforward way to make progress would be to find many more objects like them. This study represents the first step in this direction. By sifting through the massive SDSS database, we have identified a sample of AGNs that we believe are promising candidates for hosting BHs with masses below the $10^6 M_\odot$ threshold.

Our sample opens up several new avenues for further study. While well defined, our sample is likely to have missed intermediate-mass BH candidates such as NGC 4395 or POX 52, whose spectrum is dominated by narrow emission lines, with the broad-line component visible only under very high signal-to-noise ratio. Moreover, if either AGN were embedded in a much more luminous host galaxy, the weak broad lines would be even harder to discern. Furthermore, we know that pure narrow-line (type 2) AGNs do exist, either because the BLR is obscured or intrinsically absent, and there is no reason to suppose that this situation does not persist to the regime of intermediate-mass BHs. A complimentary approach, then, is to use the width of the narrow emission lines to select potential candidates. While the detailed geometry and kinematics of the narrow-line region (NLR) in AGNs are complex and not well understood, it has been argued that its velocity field is largely dominated by the gravitational potential of the bulge of the host galaxy (Smith et al. 1990; Whittle 1992a, 1992b). If so, then the velocities in the NLR are roughly virial, and on average the velocity dispersion of the line-emitting gas, σ_g , should be approximately equal to the velocity dispersion of the bulge stars, σ_* . The most detailed comparison between NLR and stellar kinematics for a large sample of Seyfert galaxies has been done by Nelson & Whittle (1996), who indeed find that in most cases $\sigma_g \approx \sigma_*$, where σ_g was measured using [O III] $\lambda 5007$. The exception are objects with powerful, jetlike radio structures where σ_g can be much larger

than σ_* , presumably because of extra nongravitational motions induced by the radio outflows. Thus, in general, one expects that σ_g , as measured in [O III] λ 5007 or other optical forbidden lines, can be taken as a rough proxy, or perhaps more realistically as an upper limit, for σ_* . We are in the process of enlarging the current sample through a selection based on this strategy.

Another important next step is to obtain stellar velocity dispersions for these objects. Such measurements will test whether the BH mass estimates we derive obey the $M_{\text{BH}}-\sigma_*$ relation. Conversely, if we assume that the $M_{\text{BH}}-\sigma_*$ relation is universally valid, the stellar velocity dispersion measurements will test the reliability of the virial mass estimator for AGNs. It would also be valuable to compare the velocity dispersions derived from stars with those derived from gas. Another area requiring attention is to obtain high-resolution, deep imaging. Much better data are needed to quantify the morphologies and detailed structural parameters of the host galaxies. Do these objects have bulges, and if so, what kind and where do they fall on galaxy scaling relations like the fundamental plane?

Finally, much work remains to be done, especially at non-optical wavelengths, to further characterize the properties of the AGNs themselves.

J. E. G. is funded by a National Science Foundation Graduate Research fellowship. L. C. H. acknowledges support by the Carnegie Institution of Washington and by NASA grants from the Space Telescope Science Institute (operated by AURA, Inc., under NASA contract NAS5-26555). We are grateful to Lei Hao for making available her PCA software, to Aaron Barth and John Huchra for helpful discussions on various aspects of this work, to Pat Hall for his timely and helpful referee's report, and to the entire SDSS collaboration for providing the extraordinary database and processing tools that made this work possible. This research has made use of data obtained from the High Energy Astrophysics Science Archive Research Center (HEASARC), provided by NASA's Goddard Space Flight Center.

REFERENCES

- Abazajian, K., et al. 2003, *AJ*, 126, 2081
 Adams, F. C., Graff, D. S., & Richstone, D. O. 2001, *ApJ*, 551, L31
 Baldwin, J. A., Phillips, M. M., & Terlevich, R. 1981, *PASP*, 93, 5
 Barth, A. J. 2004, in *Coevolution of Black Holes and Galaxies*, ed. L. C. Ho (Cambridge: Cambridge Univ. Press), in press
 Barth, A. J., Ho, L. C., Rutledge, R. E., & Sargent, W. L. W. 2004, *ApJ*, 607, 90
 Baumgardt, H., Hut, P., Makino, J., McMillan, S., & Portegies Zwart, S. 2003a, *ApJ*, 582, L21
 ———. 2003b, *ApJ*, 589, L25
 Becker, R. H., White, R. L., & Helfand, D. J. 1995, *ApJ*, 450, 559
 Bender, R., Burstein, D., & Faber, S. M. 1992, *ApJ*, 399, 462
 Blanton, M. R., et al. 2003, *ApJ*, 592, 819
 Boller, T., Brandt, W. N., & Fink, H. 1996, *A&A*, 305, 53
 Boroson, T. A. 2002, *ApJ*, 565, 78
 Bromley, J. M., Somerville, R. S., & Fabian, A. C. 2004, *MNRAS*, 350, 456
 Condon, J. J. 1992, *ARA&A*, 30, 575
 Connolly, A. J., & Szalay, A. S. 1999, *AJ*, 117, 2052
 Constantin, A., & Shields, J. 2003, *PASP*, 115, 592
 De Robertis, M. M., & Osterbrock, D. E. 1984, *ApJ*, 286, 171
 ———. 1986, *ApJ*, 301, 727
 de Vaucouleurs, G. 1948, *Ann. d'Astrophys.*, 11, 247
 Dickey, J. M., & Lockman, F. J. 1990, *ARA&A*, 28, 215
 Di Matteo, T., Croft, R. A. C., Springel, V., & Hernquist, L. 2003, *ApJ*, 593, 56
 Fabbiano, G. 1989, *ARA&A*, 27, 87
 Fabian, A. C. 2004, in *Coevolution of Black Holes and Galaxies*, ed. L. C. Ho (Cambridge: Cambridge Univ. Press), in press
 Feigelson, E. D., & Nelson, P. I. 1985, *ApJ*, 293, 192
 Ferrarese, L., & Merritt, D. 2000, *ApJ*, 539, L9
 Ferrarese, L., Pogge, R. W., Peterson, B. M., Merritt, D., Wandel, A., & Joseph, C. L. 2001, *ApJ*, 555, L79
 Filippenko, A. V. 1985, *ApJ*, 289, 475
 Filippenko, A. V., & Halpern, J. P. 1984, *ApJ*, 285, 458
 Filippenko, A. V., & Ho, L. C. 2003, *ApJ*, 588, L13
 Filippenko, A. V., Ho, L. C., & Sargent, W. L. W. 1993, *ApJ*, 410, L75
 Filippenko, A. V., & Sargent, W. L. W. 1988, *ApJ*, 324, 134
 ———. 1989, *ApJ*, 342, L11
 Francis, P. J., Hewett, P. C., Foltz, C. B., Chaffee, F. H., Weymann, R. J., & Morris, S. L. 1991, *ApJ*, 373, 465
 Fukugita, M., Ichikawa, T., Gunn, J. E., Doi, M., Shimasaku, K., & Schneider, D. P. 1996, *AJ*, 111, 1748
 Gaskell, C. M., & Ferland, G. J. 1984, *PASP*, 96, 393
 Gebhardt, K., Rich, R. M., & Ho, L. C. 2002, *ApJ*, 578, L41
 Gebhardt, K., et al. 2000a, *ApJ*, 539, L13
 ———. 2000b, *ApJ*, 543, L5
 ———. 2001, *AJ*, 122, 2469
 Gerssen, J., van der Marel, R. P., Gebhardt, K., Guhathakurta, P., Peterson, R. C., & Pryor, C. 2002, *AJ*, 124, 3270 (addendum: 2003, *AJ*, 125, 376)
 Haehnelt, M. G., Natarajan, P., & Rees, M. J. 1998, *MNRAS*, 300, 817
 Halpern, J. P., & Steiner, J. E. 1983, *ApJ*, 269, L37
 Hao, L., & Strauss, M. 2004, in *Coevolution of Black Holes and Galaxies*, ed. L. C. Ho (Pasadena: Carnegie Obs.), in press
 Ho, L. C. 1999, *ApJ*, 516, 672
 ———. 2003, *ApJ*, 583, 159
 ———. 2004a, in *Coevolution of Black Holes and Galaxies*, ed. L. C. Ho (Pasadena: Carnegie Obs.), in press
 ———. 2004b, in *Multiwavelength AGN Surveys*, ed. R. Maiolino & R. Mujica (Singapore: World Scientific), in press
 Ho, L. C., Filippenko, A. V., & Sargent, W. L. W. 1993, *ApJ*, 417, 63
 ———. 1997a, *ApJS*, 112, 315
 ———. 1997b, *ApJ*, 487, 568
 Ho, L. C., Filippenko, A. V., Sargent, W. L. W., & Peng, C. Y. 1997c, *ApJS*, 112, 391
 Ho, L. C., & Peng, C. Y. 2001, *ApJ*, 555, 650
 Ho, L. C., Rudnick, G., Rix, H.-W., Shields, J. C., McIntosh, D. H., Filippenko, A. V., Sargent, W. L. W., & Eracleous, M. 2000, *ApJ*, 541, 120
 Ho, L. C., & Ulvestad, J. S. 2001, *ApJS*, 133, 77
 Ho, L. C., et al. 2001, *ApJ*, 549, L51
 Hughes, S. A. 2002, *MNRAS*, 331, 805
 Islam, R. R., Taylor, J. E., & Silk, J. 2003, *MNRAS*, 340, 647
 Kaspi, S., Smith, P. S., Netzer, H., Maoz, D., Jannuzi, B. T., & Giveon, U. 2000, *ApJ*, 533, 631
 Kauffmann, G., et al. 2003, *MNRAS*, 346, 1055
 Köhler, T., Groote, D., Reimers, D., & Wisotzki, L. 1997, *A&A*, 325, 502
 Koushiappas, S. M., Bullock, J. S., & Dekel, A. 2004, *MNRAS*, submitted (astro-ph/0311487)
 Kraemer, S. B., Ho, L. C., Crenshaw, D. M., Filippenko, A. V., & Shields, J. C. 1999, *ApJ*, 520, 564
 Krolik, J. H. 2001, *ApJ*, 551, 72
 Kunth, D., Sargent, W. L. W., & Bothun, G. D. 1987, *AJ*, 93, 29
 Kwan, J., & Krolik, J. H. 1981, *ApJ*, 250, 478
 Lupton, R. H., Gunn, J. E., & Szalay, A. S. 1999, *AJ*, 118, 1406
 Magorrian, J., et al. 1998, *AJ*, 115, 2285
 Malkan, M. A. 1988, *Adv. Space Res.*, 8, 49
 McLure, R. J., & Dunlop, J. S. 2004, *MNRAS*, in press (astro-ph/0310267)
 Moore, B., Katz, N., Lake, G., Dressler, A., & Oemler, A. 1996, *Nature*, 379, 613
 Moran, E. C., Filippenko, A. V., Ho, L. C., Shields, J. C., Belloni, T., Comastri, A., Snowden, S. L., & Sramek, R. A. 1999, *PASP*, 111, 801
 Moran, E. C., Eracleous, M., Leighly, K. M., Chartas, G., Filippenko, A. V., Ho, L. C., & Blanco, P. R. 2004, *ApJ*, submitted
 Nagar, N. M., Falcke, H., Wilson, A. S., & Ulvestad, J. S. 2002, *A&A*, 392, 53
 Nelson, C. H., & Whittle, M. 1996, *ApJ*, 465, 96
 Osterbrock, D. E., & Pogge, R. W. 1985, *ApJ*, 297, 166
 Osterbrock, D. E., & Shuder, J. M. 1982, *ApJS*, 49, 149
 Pelat, D., Alloin, D., & Fosbury, R. A. E. 1981, *MNRAS*, 195, 787
 Pounds, K. A., Done, C., & Osborne, J. P. 1995, *MNRAS*, 277, L5
 Richards, G. T., et al. 2002, *AJ*, 123, 2945
 Richstone, D. 2004, in *Coevolution of Black Holes and Galaxies*, ed. L. C. Ho (Cambridge: Cambridge Univ. Press), in press

- Schneider, R., Ferrara, A., Natarajan, P., & Omukai, K. 2002, *ApJ*, 571, 30
- Sheth, R. K., et al. 2003, *ApJ*, 594, 225
- Shields, J. C., Rix, H.-W., McIntosh, D. H., Ho, L. C., Rudnick, G., Filippenko, A. V., Sargent, W. L. W., & Sarzi, M. 2000, *ApJ*, 534, L27
- Shih, D. C., Iwasawa, K., & Fabian, A. C. 2003, *MNRAS*, 341, 973
- Shimasaku, K., et al. 2001, *AJ*, 122, 1238
- Smith, E. P., Heckman, T. M., & Illingworth, G. D. 1990, *ApJ*, 356, 399
- Smith, J. A., et al. 2002, *AJ*, 123, 2121
- Sołtan, A. 1982, *MNRAS*, 200, 115
- Stoughton, C., et al. 2002, *AJ*, 123, 485
- Strateva, I., et al. 2001, *AJ*, 122, 1861
- Terashima, Y., & Wilson, A. S. 2003, *ApJ*, 583, 145
- Tremaine, S., et al. 2002, *ApJ*, 574, 740
- van der Marel, R. P. 2004, in *Coevolution of Black Holes and Galaxies*, ed. L. C. Ho (Cambridge: Cambridge Univ. Press), in press
- Veilleux, S., & Osterbrock, D. E. 1987, *ApJS*, 63, 295
- Véron-Cetty, M.-P., Véron, P., & Gonçalves, A. C. 2001, *A&A*, 372, 730
- Volonteri, M., Haardt, F., & Madau, P. 2003, *ApJ*, 582, 559
- Whittle, M. 1985, *MNRAS*, 213, 1
- . 1992a, *ApJ*, 387, 109
- . 1992b, *ApJ*, 387, 121
- Williams, R. J., Pogge, R. W., & Mathur, S. 2002, *AJ*, 124, 3042
- Wrobel, J. M., Fasnacht, C. D., & Ho, L. C. 2001, *ApJ*, 553, L23
- York, D. G., et al., 2000, *AJ*, 120, 1579
- Yu, Q., & Tremaine, S. 2002, *MNRAS*, 335, 965